Journal of Radiation Research and Applied Sciences 15 (2022) 100485

Contents lists available at ScienceDirect

Journal of Radiation Research and Applied Sciences

journal homepage: www.journals.elsevier.com/journal-of-radiation-research-and-applied-sciences

The impacts of colors on the catalyst HD system: Gains, integral times, and setups in radiotherapy

Haiyan Peng [a,1], Fu Jin [b,*,1], Chao Li [a], Huanli Luo [a], Qiang Liu [c,**], Yang He [a], Kaijin Mao [a], Juan Zhou [d]

[a] Department of Radiation Oncology, Chongqing University Cancer Hospital, Chongqing, 400030, China
[b] Department of Radiation Oncology, Chongqing University Cancer Hospital, No. 181 Hanyu Road, Shapingba District, Chongqing, 400030, China
[c] Department of Radiation Oncology, Chongqing University Three Gorges Hospital, Chongqing, 404000, China
[d] College of Criminal Investigation, Southwest University of Political Science and Law, Chongqing, China

ARTICLE INFO

Keywords:
Surface monitoring system
Radiotherapy
Catalyst HD
Color
Setup error

ABSTRACT

Purpose: To build an image-scanning protocol of Catalyst HD and to investigate the impacts of different colors on gains (G_a), integral times (T_i), and setups using this system.
Methods: Thirty-eight cards with different skin tones were studied, and the color difference ΔE was calculated based on a reference color in the RGB (R: red, G: green, B: blue) space. Correlations were investigated among ΔE, G_a, and T_i. After routine setup verification, the card position changed from −5 mm to 5 mm with a step size of 2 mm, and they were measured by Catalyst HD simultaneously. The position differences were calculated to evaluate setup errors.
Results: As G_a changed from 100% to 1000%, the natural logarithmic function of T_i (lnT_i) linearly decreased with a constant slope of −0.002. If the reference color had an RGB value of (200, 172, 153), lnT_i increased linearly with slopes of 0.006 and 0.007 for the main and side cameras respectively, as ΔE increased. Moreover, there were significant positive correlations between measured positions and true values. The correlation coefficient r_{pos} changed as a sigmoid function of ΔE. There was a ΔE threshold of 254.0 for color detection. The detection was different for different colors. Additionally, r_{pos} depended on the RGB values, curvature, edge and area of a region-of-interest.
Conclusions: There are close correlations among ΔE, G_a, and T_i, and ΔE has an impact on setup accuracy using Catalyst HD.

1. Introduction

In recent years, oncologists are trying to gather more information through some advanced technologies to make the optimal choices for individual patients, in the hopes of making clinical practices faster, more accurate, more comfortable, and more economic (i.e. "FACE" principle) (Shulman et al., 2020). Driven by this principle and given the features of conventional cone-beam computed tomography (CBCT) including time-consuming, additional doses, and being unable to monitor setup errors, optical surface monitoring systems (OSMSs) have been widely adopted in radiotherapy (RT) for several cancers to identify and track the position of a patient's external surface, such as setup, gating and monitoring (Benkhaled et al., 2022; Han et al., 2022; Nankali et al., 2022). These clinical practices show promising results in reducing setup errors and improving patient positioning monitoring, especially for anatomical sites in which the patient's surface is a good surrogate for the RT target.

However, the application of OSMS is affected by image qualities and surface characteristics such as shape, location, and materials (Song et al., 2022). Recently, a report of the American Association of Physicists in Medicine (AAPM) commissioned Task Group 302 provided some

Peer review under responsibility of The Egyptian Society of Radiation Sciences and Applications.
* Corresponding author.
** Corresponding author.
E-mail addresses: penghaiyan_cq@163.com (H. Peng), jfazj@126.com (F. Jin), creat_1986@163.com (C. Li), luohuanli_cq@126.com (H. Luo), lqlq_liuqiang@126.com (Q. Liu), heyang_cq@163.com (Y. He), zhengxd018@126.com (K. Mao), zjajf@126.com (J. Zhou).
[1] **Co-first authors:** Fu Jin and Haiyan Peng.

https://doi.org/10.1016/j.jrras.2022.100485
Received 31 July 2022; Received in revised form 23 October 2022; Accepted 14 November 2022
Available online 21 November 2022

List of abbreviations

G_a	gain
T_i	integral time
ΔE	color difference
R	red
G	green
B	blue
lnT_i	the natural logarithmic function of T_i
r_{pos}	the Pearson correlation coefficient between measured positions and true values
"FACE"	faster, more accurate, more comfortable, and more economic
CBCT	cone-beam computed tomography
OSMS	optical surface monitoring system
RT	radiotherapy
AAPM	American Association of Physicists in Medicine
Y	yellow
AP	anterior–posterior
LR	left–right
SI	superior–inferior
DIBH	deep inspiration breath-hold

technical guidelines and quality assurance requirements, and it also recommended to assess the effect of surface characteristics on localization accuracy (Al-Hallaq et al., 2022). But how to qualify the impact of image qualities and surface characteristics and how much of this impact are absent in this report. In order to better serve the clinical practices, a strategy to select exposure parameters was developed to get the optimal image qualities based on a reference color in the RGB (R: red, G: green, B: blue) space in this study. According to this strategy, surface images were scanned and the effect of image qualities and surface characteristics on localization accuracy was assessed by testing different toned cards. Additionally, the impact of light intensities on both exposure parameters and setup accuracy was studied in different scenarios.

2. Materials and methods

2.1. Catalyst HD and SkinTone

The Catalyst HD system (C-RAD, Uppsala, Sweden) employs optical triangulation to obtain patient surface information, and three cameras are ceiling-mounted in the RT treatment room. Two optical parameters, gain (G_a) and integral time (T_i) should be set. G_a is the ratio of the number of captured electrons by the camera to a digital readout and T_i is the time of light absorption. In this study, the main camera was installed a year earlier than the side cameras, and all commissioning procedures were based on the AAPM task group report 147 (Willoughby et al., 2012).

To get a uniform and consistent color, the Pantone STG-201 (Pantone SkinTone Guide, United States) was used to represent skin color (Fig. 1a). One hundred and ten color cards are numbered from 1Y01 to 4R15 (Y: yellow, R: red), comprised of a four-digit alpha numeric number (Fig. 1b). The first two positions reflect the hue, and the others represent brightness. The dimensions of each card are 4.44 cm × 17.78 cm. In this study, twenty kinds of colors were chosen randomly to investigate the impact of color on G_a and T_i, and twenty-four were used to measure setup errors using Catalyst HD (Fig. 1f).

2.2. Gain, integral time, and setup errors

All cards were attached to the top of a cylindrical phantom with a radius of 15 cm to investigate the impact of different colors on G_a, T_i, and setup errors (Fig. 1c). Meanwhile, an image-scanning protocol was proposed to optimize the camera settings for maximum card surface visibility, i.e., G_a was sequentially set from 100% to 1000% with a step size of 100%, and T_i (μs) was adjusted simultaneously. Once red

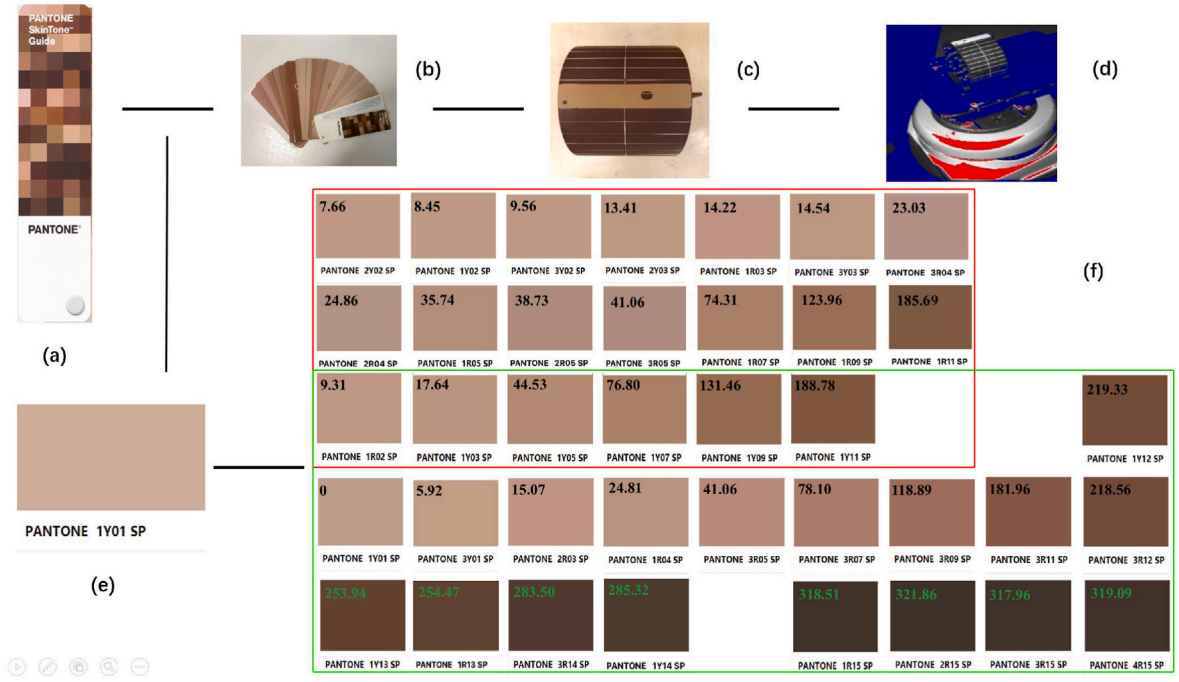

Fig. 1. The illustrations of Pantone SkinTone cards and the image-scanning protocol. (a) The Pantone STG-201. (b) One hundred and ten color cards. (c) A card was attached to the top of a cylindrical phantom longitudinally. (d) Both gain and integral time were adjusted to make red overexposures just appear in the periphery of the card. (e) The reference color 1Y01, R = 200, G = 172, and B = 153. (f) Twenty colors in the red box were chosen to investigate the impact of colors on gain and integral time; twenty-four colors in the green box were used to measure setup errors. The value on each color was the corresponding color difference ΔE based on the reference color 1Y01. (For interpretation of the references to color in this figure legend, the reader is referred to the Web version of this article.)

overexposures just appear in the periphery of the card, the pair of G_a and T_i was the optimal exposure parameter (Fig. 1d). By switching on different lighting sets, we could obtain different background luminances. The intensity of background light was measured by digital Lux meter (PP720, SanLiang, Janpan) and it increased from 0.0 Lux to 184.3 Lux, i.e., 0.0 Lux, 42.2 Lux, 69.4 Lux, 76.9 Lux, 127.5 Lux, 135.0 Lux, 141.5 Lux, and 184.3 Lux. Both G_a and T_i were measured repeatedly under different lighting conditions.

The routine setup of the phantom was performed with an on-board imager via CBCT verification. After verification, the following surface scan was regarded as a reference image. Thereafter, the phantom randomly moved from −5 mm to 5 mm with a step size of 2 mm, and the position was measured by Catalyst HD simultaneously through registering the current surface image with the reference image. The differences between measured positions and true values were calculated to evaluate setup errors. Positive values for the left–right (LR), superior–inferior (SI) and anterior–posterior (AP) indicated motion in the left, cranial and posterior directions, respectively. When the phantom was placed longitudinally, the position couldn't be detected in the SI direction because there was no curvature (Fig. 1d). Measurements should be repeated in this direction when the phantom was placed laterally. Before every measuring, daily checking was performed. Both thermal equilibrium and system drift were taken into account.

In order to further get the impacts of curvatures on setup errors, the cards were attached to the top of a flat treatment couch. Due to the fixed edge length of a card, setup dependences on edge and area were tested by cutting a piece of white printer paper into many pieces with different dimensions, i.e., 2 cm × 2 cm, 2 cm × 21 cm, 3 cm × 3 cm, 3 cm × 21 cm, 4 cm × 4 cm, 4 cm × 21 cm, 5 cm × 5 cm, 6 cm × 6 cm, and 7 cm × 7 cm.

2.3. Data analysis

The color difference ΔE was calculated based on a reference color 1Y01 (the lightest yellow in the STG-201) using equations (1)–(5) (Mokrzycki, 2011). $C_{1,R}$ and $C_{2,R}$ represent R values of two kinds of colors; $C_{1,G}/C_{2,G}$ and $C_{1,B}/C_{2,B}$ represent G and B values respectively. The correlations among G_a, T_i, and ΔE were assessed using linear regression analysis. Meanwhile, the impact of different reference color on these correlations was tested when 4R15 SP (the deepest color of this study) was used as the new reference color. The regression analysis was repeated.

$$\bar{r} = \frac{C_{1,R} + C_{2,R}}{2} \tag{1}$$

$$\Delta E = \sqrt{\left(2 + \frac{R+200}{512}\right) \times (R-200)^2 + 4 \times (G-172)^2 + \left(\frac{767}{256} - \frac{R+200}{512}\right) \times (B-153)^2} \tag{8}$$

$$\Delta R = C_{1,R} - C_{2,R} \tag{2}$$

$$\Delta G = C_{1,G} - C_{2,G} \tag{3}$$

$$\Delta B = C_{1,B} - C_{2,B} \tag{4}$$

$$\Delta E = \sqrt{\left(2 + \frac{\bar{r}}{256}\right) \times \Delta R^2 + 4 \times \Delta G^2 + \left(2 + \frac{255 - \bar{r}}{256}\right) \times \Delta B^2} \tag{5}$$

A comparison of the true position with the measured value was performed using the paired *t*-tests. The Pearson correlation coefficient (r_{pos}) between them was calculated. The dependences of both r_{pos} and setup errors on ΔE were analyzed. Statistical analyses were performed using IBM SPSS statistics (version22, IBM Corporation, Armonk, NY, USA). $P < 0.05$ was considered statistically significant.

3. Results

3.1. Gain, integral time, and color difference

When G_a was less than 400%, the image-scanning protocol couldn't be satisfied by the main camera for 1R11 and 1Y11 as T_i increased. Once T_i reached the maximum value 50000μs, the red overexposures immediately appeared in the entire scanning surface. Hence, there were missing data points in Figs. 2 and 3. Otherwise, all other cases satisfied the scanning protocol.

If the 1Y01 card (200, 172, 153) was chosen as a reference color, lnTi linearly decreased with a constant slope of −0.002 as G_a changed from 100% to 1000%. For example, Fig. 2 showed $\ln T_i$ as a function of G_a together with a linear fit for two cases, ΔE = 7.66 and ΔE = 188.78, and the fitting parameter p1 was −0.002 with a fitting probability of 1. This result was consistent between the main camera and the side ones. Also $\ln T_i$ increased linearly as ΔE increased, but the slope was different between the main camera and the side ones. Fig. 3 showed $\ln T_i$ as a function of ΔE when G_a = 100% and G_a = 1000%. The fitting parameter p1 was 0.006–0.007 for side cameras, and 0.004–0.006 for the main camera with a fitting probability of 1. Meanwhile, the fitting parameters were different between yellow and red colors. All fitting figures can be found in the supplementary files.

If the red and yellow colors were combined, the relationships among T_i, G_a, and ΔE could be delineated by the following equations (6)–(8) after linear regression analysis, where $T_{i,main}$, $T_{i,side}$, $G_{a,main}$, and $G_{a,side}$ were integral time and gain for the main camera and the side ones, respectively. If red and yellow data points were analyzed separately, the intercepts of the main and side cameras were 10.37 and 8.922 for yellow colors; as for red colors, the intercepts were 10.32 and 8.945, respectively. However, if the reference color changed into 4R15 (84, 66, 57), the relationship could not be delineated by those linear equations. Additionally, when the light intensity increased from 0 Lux to 184.3 Lux, $\ln T_i$ was reduced and the maximum deviation of 0.37% was achieved when G_a was1000%.

$$\ln T_{i,main} = 10.350 - 0.002 G_{a,main} + 0.006 \Delta E \tag{6}$$

$$\ln T_{i,side} = 8.935 - 0.002 G_{a,side} + 0.007 \Delta E \tag{7}$$

v

3.2. Setup errors and color difference

There were significant positive correlations between measured positions and true values ($P < 0.05$). This correlation (r_{pos}) depended on ΔE, and the dependence could be delineated by a sigmoid model (Fig. 4):

$$r_{pos} = \frac{1}{1 + e^{p_0 \times (\Delta E - p_1)}} \tag{9}$$

where both p_0 and $p_1$were the fitting parameters. When four cards (1Y13, 1R13, 3R14, and 1Y14) were scanned, their positions were not be monitored stably, so these colors were not involved in the curve fitting, seen in Fig. 4 (vertical lines and arrows, ΔE = 254.0). As for another four colors (1R15, 2R15, 3R15, and 4R15) in Fig. 1f, the Catalyst HD couldn't get their images, so r_{pos} was set to 0.001 when ΔE was larger than 318.0.

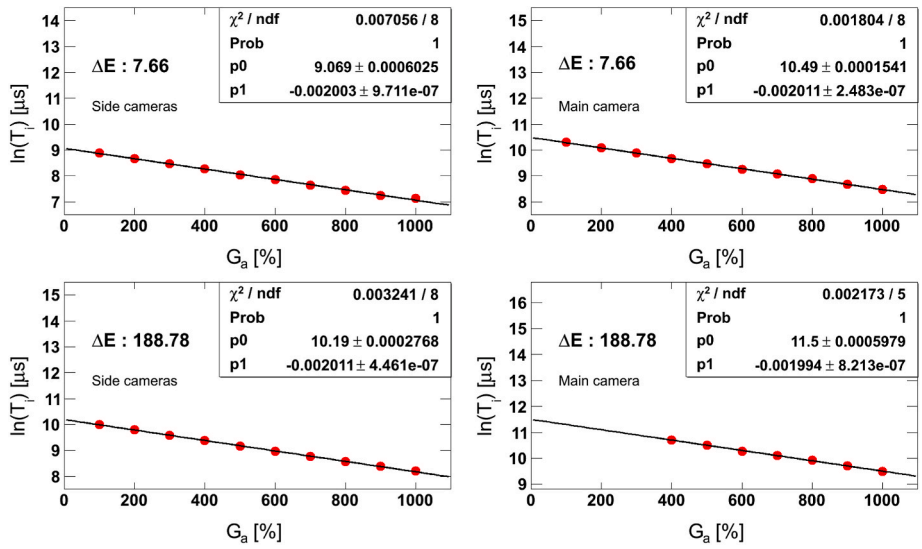

Fig. 2. The natural logarithmic function of integral time as a function of gain together with a linear fit for two cases, ΔE = 7.66 and ΔE = 188.78. There were some missing data points for the main camera when the color difference was 188.78 and gain was less than 400%. (For interpretation of the references to color in this figure legend, the reader is referred to the Web version of this article.)

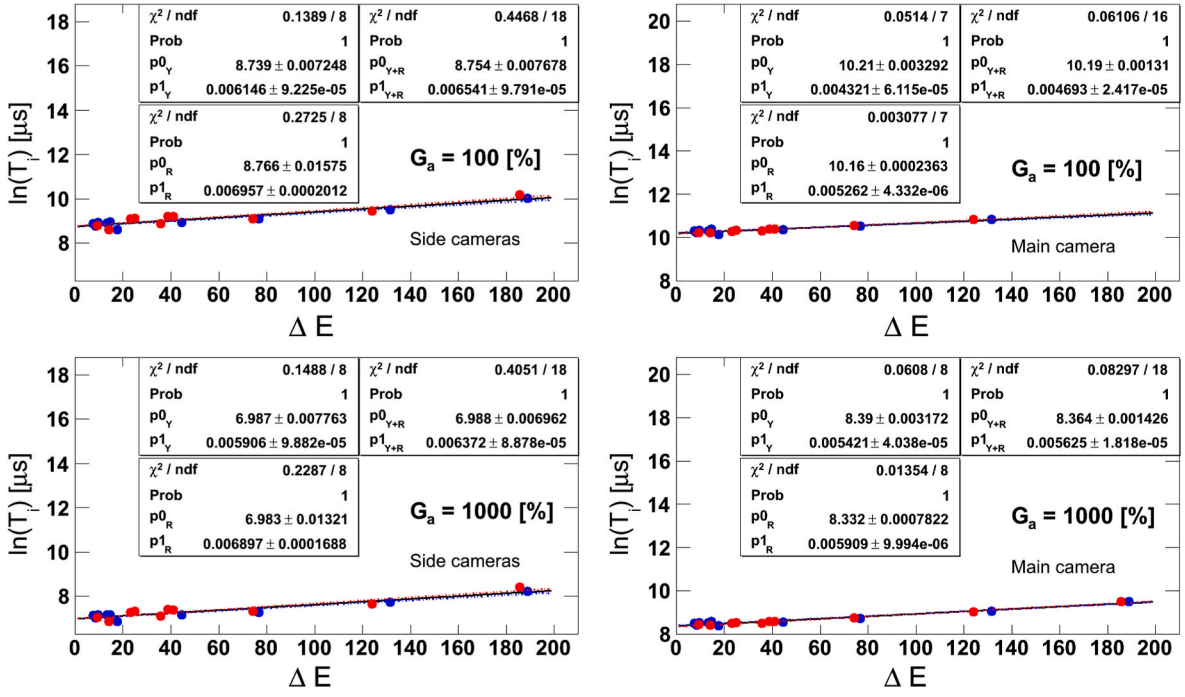

Fig. 3. The natural logarithmic function of integral time as a function of color difference together with a linear fit when Ga = 100% and Ga = 1000%. Red points: red colors; blue points: yellow colors; black lines: the fitting curves of combined yellow and red data points (Y + R); red lines: only red colors (R); blue lines: only yellow colors (Y). There were some missing data points for the main camera when gain was 100%. (For interpretation of the references to color in this figure legend, the reader is referred to the Web version of this article.)

Changing these settings did not affect the fitting results.

As shown in Fig. 4, the steepness of the sigmoid curve was the largest in the AP direction, and the yellow color showed bigger steepness than the red one in the LR and SI directions. In addition, the detection of white color (black star) was different from both yellow colors and red ones.

Meanwhile, the bottom of Fig. 4 showed mean difference between measured position and true value as a function of ΔE. When ΔE was less than 132.0, uncertainties were small in the LR and SI directions, and the mean setup error was smaller than 1 mm except ΔE of 131.5 in the LR direction. There were 37.5%, 62.5%, 93.8% of setup errors smaller than 0.5 mm, and 43.8%, 25.0%, 6.2% of errors larger than 0.5 mm and smaller than 1 mm in the LR, SI, and AP directions, respectively. Mean setup errors were the smallest in the AP direction, and the detection in AP was superior to that in the others.

Moreover, both r_{pos} and setup errors depended on R, G, B, and ΔE. The correlation coefficients between r_{pos} and the above color parameters were 0.862, 0.855, 0.813, and −0.921 ($P = 0.00$) in the LR direction, 0.673, 0.711, 0.646, and −0.769 ($P < 0.01$) in the SI direction, and 0.649, 0.653, 0.664 ($P < 0.01$) and −0.456 ($P = 0.076$) in the AP

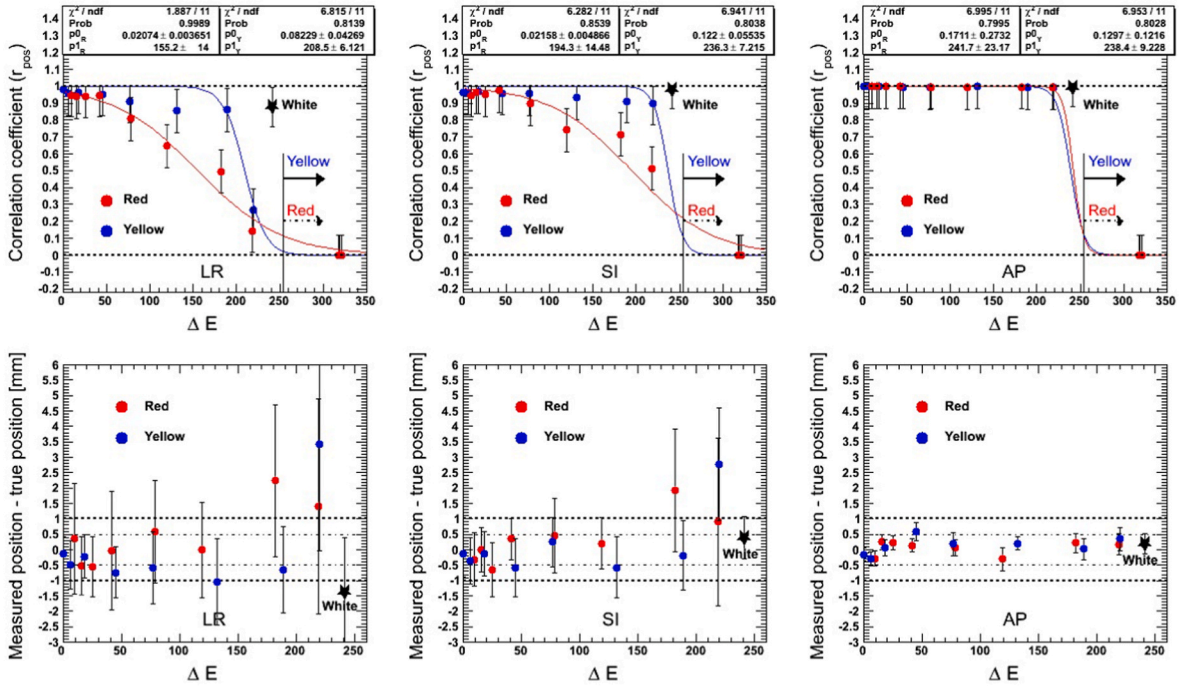

Fig. 4. The top images: r_{pos} as a function of color difference together with a non-linear fit. Arrows mean undetectable color differences; vertical bars are error bars; red line: red color fitting (R); blue line: yellow color fitting (Y). The bottom images: mean difference between measured position and true value as a function of color difference. Vertical bars mean the uncertainties. Dash lines: $-1 \leq$ values ≤ 1; dash-dotted lines: $-0.5 \leq$ values ≤ 0.5. Red points: red colors; blue points: yellow colors; black star: white color. (For interpretation of the references to color in this figure legend, the reader is referred to the Web version of this article.)

direction, respectively. Similarly, the correlation coefficients between mean setup errors and color parameters were −0.638, −0.619, −0.569, and 0.786 ($P < 0.02$) in the LR direction, −0.683, −0.683, −0.64, and 0.772 ($P < 0.01$) in the SI direction, and −0.288, −0.269, −0.29 and 0.142 ($P > 0.28$) in the AP direction, respectively.

In addition, r_{pos} also depended on curvature, edge, and area. Its value was almost zero in the LR and SI directions, but larger than 0.99 in the AP direction when the curvature was zero. Only if the length of short edge of a rectangle was ≥4 cm or the length of a square was >5 cm, the image of a region of interest could be captured and the setup error could be evaluated using a non-rigid algorithm. Moreover, r_{pos} increased with increasing edge and area in a specific direction where the curvature was not zero.

4. Discussion

The OSMS is a non-ionizing and non-invasive optical scanning system. It has many attractive features for setup, monitoring and respiratory gating during RT. The previous researches mainly focused on the positioning difference among cross-line laser, CBCT and OSMS techniques. Early in 2014, Wikström Ket al. found that mean difference between OSMS and CBCT was ≤0.1 mm for pelvic targets (Wikström et al., 2014). For rectal cancer, a significant different was observed between laser and OSMS only in the lateral direction (median, 2.0 cm vs. 1.3 cm) (Hamid, 2017). OSMS also presented an accuracy of 0.3 mm for displacements up to 1 cm for cranial lesions (Mancosu et al., 2016). Additionally, OSMS could detect swallowing, incorrect arm and shoulder positions, or provide accurate tracking of thoracoabdominal surface coupled with other techniques such as deep inspiration breath hold (DIBH) (Mcconnell et al., 2021). All these studies indicate that OSMS is a good supplement to the conventional system for accurate RT setup.

However, due to the projected and reflected patterns of colored light on the surface, OSMSs depend on the surface optical absorbance and reflectance properties, which can vary with surface shape and color (Stieler et al., 2013). The OSMS detection also depended on the surface imaging quality. Recently, the task group report 302 provided some technical guidelines and quality assurance requirements, but how to qualify the impact of image qualities and surface characteristics and how much of this impact were absent in this report (Al-Hallaq et al., 2022).

Considering all these aspects together, we first proposed an image-scanning protocol according to the vendor's suggestions and our measured experiences in this article, and then the relationships between exposure parameters and ΔE were delineated by equations (6)–(8). Based on these equations, therapists can calculate G_a and T_i and set their default values, given the patient's skin color. The skin color can be measured using SkinColorCatch (Delfin Technologies Ltd, Finland) at the planning CT scan. This operation will undoubtedly improve the work efficiency, and improve the image qualities. In this study, there were some differences between the main camera and the side ones. The main camera required more integration time than the side cameras using the same gain. A mean T_i of 4220 μs or 16376 μs was used for the side cameras or the main camera, respectively. It might be caused by production aging or batch because the main camera was installed a year earlier than the side cameras.

Additionally, both Figs. 2 and 3 and equations (6)–(8) showed that the darker the surface was and the higher T_i or G_a has to be. For dark colors in this study, i.e., 1R11 and 1Y11, the images couldn't be captured by the main camera when G_a was lower than 400%. But the surface images and setup errors could be obtained stably if G_a was ≥400%. For extremely dark colors, i.e., 1R15, 2R15, 3R15, and 4R15, the detection could not be completed because there was not enough light to reflect. Moreover, gain adjustments might lead to increased noises (Wang et al., 2012). Hence, a gain of 400% was adopted in the following analysis of setup errors.

Tumor motion management strategies play an important role in the thoracic and abdominal RT. Many surrogate-based motion models are constructed by correlating motion of an external surrogate and internal anatomy to guide motion management (Steiner et al., 2019). For breast cancer, a superior correlation was observed between the surface imaging and the actual target positioning during DIBH (Rong et al., 2014). The

surface image was demonstrated as a superior surrogate. However, skin color changed during RT. Higher RT dose made skin darker and redder (Yamazaki et al., 2018). Hence, we must pay attention to the color dependence of setup error.

As it is mentioned above, yellow colors showed bigger steepness than red colors in the LR and SI directions. Hence, the detection of Catalyst HD became worse as skin turned red. Also the detection performance decreased as RT doses increased. There was no doubt that the skin surface would not be monitored when the color difference reached a certain threshold. In this study, we found that the surface was completely unable to observe when ΔE was 254.0 based on 1Y01. Hence, in our center, we are trying to establish a skin management protocol to dynamically evaluate skin changes using Delfin products during surface-image guided RT.

Meanwhile, the setup accuracy changed with different colors, and this trend was the most obvious in the LR direction, shown in the top of Fig. 4. The correlation coefficient r_{pos} changed with a sigmoid distribution. The detection of Catalyst HD was almost unaffected by color changes in the AP direction when ΔE was smaller than 219.3 based on 1Y01. If ΔE was greater than this value, r_{pos} dropped rapidly in the AP direction. This curve was close to the one of a staircase function. It demonstrated an excellent detection in the AP direction. Given that motion in the AP direction is the main source of patient position variability in some cancers (Apicella et al., 2016; Ricotti et al., 2017), Catalyst HD can be used for accurate motion management.

In addition, the detection of Catalyst HD also depended on curvature, but the dependence didn't occur in the AP direction. It once again demonstrated the excellent monitoring capabilities of Catalyst HD in the AP direction. Moreover, we found that the setup errors could be evaluated accurately only if the length of short edge of a rectangle was $\geq$4 cm or the length of a square was >5 cm. The dependence on edge or area was also observed. It meant that the choice of a region of interest was crucial during surface-image guided RT.

5. Conclusion

The application of OSMS is affected by image qualities and surface characteristics. In order to improve the image quality, we proposed an image-scanning protocol through changing G_a and T_i. A linear function among $\ln T_i$, G_a, and ΔE was observed. Based on this function, therapists can initialize G_a and T_i according to skin colors to improve RT efficiency. In addition, the detection of Catalyst HD depended on R, G, B, ΔE, edge, area and curvature. It was different between different colors. The detection dependence on ΔE changed with a sigmoid distribution. In the AP direction, the distribution was close to a staircase function and the dependence on curvature was not found. Hence, it is feasible to manage motion accurately by Catalyst HD.

Ethics approval and consent to participate

Not applicable.

Consent for publication

Not applicable.

Authors' contributions

Haiyan Peng and Fu Jin participated in the design of the study and performed the statistical analysis, Chao Li, Huanli Luo, Qiang Liu, Yang He, Kaijin Mao, and Juan Zhou participated in the data collection, Fu Jin and Qiang Liu conceived of the study, and participated in its design and coordination and helped to draft the manuscript, All authors read and approved the final manuscript.

Funding

This work was partially supported by Chongqing medical scientific research project (Joint project of Chongqing Health Commision and Science and Technology Bureau) under Grant No. 2022DBXM005, Chongqing Technology Innovation and application demonstration project (No.cstc2018jscx-msybX0115), and the National Natural Science Foundation of China under Grant No. 11805025.

Declaration of competing interest

The authors have no relevant conflicts of interest to disclose.

Acknowledgements

The authors thank the following colleagues for their assistance and advice in this study: Baozhong Liang, Xia Tan, Jiaojiao Luo, Panpan Cao, and Mengfan Sun. This work was partially supported by Chongqing medical scientific research project (Joint project of Chongqing Health Commision and Science and Technology Bureau) under Grant No. 2022DBXM005, Chongqing Technology Innovation and application demonstration project (No.cstc2018jscx-msybX0115), and the National Natural Science Foundation of China under Grant No. 11805025.

Appendix A. Supplementary data

Supplementary data to this article can be found online at https://doi.org/10.1016/j.jrras.2022.100485.

References

Al-Hallaq, H. A., Cerviño, L., Gutierrez, A. N., et al. (2022). AAPM task group report 302: Surface-guided radiotherapy. *Medical Physics, 49*(4), e82–e112.

Apicella, G., Loi, G., Torrente, S., et al. (2016). Three-dimensional surface imaging for detection of intra-fraction setup variations during radiotherapy of pelvic tumors. *Radiologia Medica, La, 121*(10), 805–810.

Benkhaled, S., Gomes da Silveira Cauduro, C., Jullian, N., et al. (2022). Inter-fraction heart displacement during voluntary deep inspiration breath hold radiation therapy without visual feedback measured by daily CBCT. *Frontiers Oncology, 12*, Article 936088.

Hamid, S. (2017). *A comparison of surface based and laser based setup for rectal cancer patients in radiotherapy*.

Han, C., Amini, A., Wong, J. Y. C., et al. (2022). Comparison of intrafractional motion with two frameless immobilization systems in surface-guided intracranial stereotactic radiosurgery. *Journal of Applied Clinical Medical Physics, 23*(6), Article e13613.

Mancosu, P., Fogliata, A., Stravato, A., Tomatis, S., Cozzi, L., & Scorsetti, M. (2016). Accuracy evaluation of the optical surface monitoring system on EDGE linear accelerator in a phantom study. *Medical Dosimetry, 41*(2), 173–179.

Mcconnell, K., Kirby, N., Rasmussen, K., et al. (2021). Variability of breast surface positioning using an active breathing coordinator for aDeep inspiration breath hold technique. *Cureus, 13*(6), Article e15649.

Mokrzycki, W. S. (2011). TatolM.Color difference ΔE -A survey. *Machine Graphics and Vision, 20*, 383–411.

Nankali, S., Hansen, R., Worm, E., et al. (2022). Accuracy and potential improvements of surface-guided breast cancer radiotherapy in deep inspiration breath-hold with daily image-guidance. *Physics in Medicine and Biology, 67*(19). https://doi.org/10.1088/1361-6560/ac9109

Ricotti, R., Ciardo, D., Fattori, G., et al. (2017). Intra-fraction respiratory motion and baseline drift during breast Helical Tomotherapy. *Radiotherapy & Oncology, 122*(1), 79–86.

Rong, Y., Walston, S., Welliver, M. X., Chakravarti, A., & Quick, A. M. (2014). Improving intra-fractional target position accuracy using a 3D surface surrogate for left breast irradiation using the respiratory-gated deep-inspiration breath-hold technique. *PLoS One, 9*(5), Article e97933.

Shulman, L. N., Sheldon, L. K., & Benz, E. J. (2020). The future of cancer care in the United States-overcoming workforce capacity limitations; comment: Fu Jin. Regional partnerships in cancer prevention and treatment. *JAMA Oncology, 6*(3), 327–328.

Song, Y., Zhai, X., Liang, Y., Zeng, C., Mueller, B., & Li, G. (2022). Evidence-based region of interest (ROI) definition for surface-guided radiotherapy (SGRT) of abdominal cancers using deep-inspiration breath-hold (DIBH) [published online ahead of print, 2022 Aug 10]. *Journal of Applied Clinical Medical Physics*, Article e13748.

Steiner, E., Shieh, C. C., Caillet, V., et al. (2019). Both four-dimensional computed tomography and four-dimensional cone beam computed tomography under-predict lung target motion during radiotherapy. *Radiotherapy & Oncology, 135*, 65–73.

Stieler, F., Wenz, F., Shi, M., & Lohr, F. (2013). A novel surface imaging system for patient positioning and surveillance during radiotherapy. A phantom study and clinical evaluation. *Strahlentherapie und Onkologie, 189*(11), 938–944.

Wang, D., Zhang, T., & Kuang, H. (2012). Relationship between the charge-coupled device signal-to-noise ratio and dynamic range with respect to the analog gain. *Applied Optics, 51*(29), 7103–7114.

Wikström, K., Nilsson, K., Isacsson, U., & Ahnesjö, A. (2014). A comparison of patient position displacements from body surface laser scanning and cone beam CT bone registrations for radiotherapy of pelvic targets. *Acta Oncologica, 53*(2), 268–277.

Willoughby, T., Lehmann, J., Bencomo, J. A., et al. (2012). Quality assurance for nonradiographic radiotherapy localization and positioning systems: Report of task group 147. *Medical Physics, 39*(4), 1728–1747.

Yamazaki, H., Takenaka, T., Aibe, N., et al. (2018). Comparison of radiation dermatitis between hypofractionated and conventionally fractionated postoperative radiotherapy: Objective, longitudinal assessment of skin color. *Scientific Reports, 8*(1), Article 12306.